Transmission Electron Diffraction Intensities from Real Organic Crystals: Thin Plate Microcrystals of Paraffinic Compounds

Douglas L. Dorset

Molecular Biophysics Department, Medical Foundation of Buffalo, New York

Z. Naturforsch. **33a**, 964–982 (1978); received March 1, 1978

Solvent-grown microcrystals of long polymethylene compounds packing in the $O_\perp$ methylene subcell are found to have some of the defect structures seen for crystalline polyethylene. Crystals composed either of rectangular layers or of oblique layers both exhibit the growth around a screw dislocation characterized earlier by other workers. In addition, rectangular layer crystals of orthorhombic n-hexatriacontane give evidence of *intra*lamellar edge dislocations. When rectangular layer crystals of cetyl palmitate are grown from hot ethanol, the same surface corrugations are found as seen earlier for polyethylene and orthorhombic paraffins. Oblique layer crystals have not demonstrated these latter two defect structures. All crystals show evidence of appreciable bending.

As was found to be true for rectangular layers of n-paraffins, bending has some influence on the electron diffraction intensities from an oblique layer. Another important factor is a perturbation due to defects along long chain axes which disrupts the ordered packing of polar regions, and causes incoherent scatter from these regions. In addition, observed screw dislocations give a nonuniform end plane, causing isolation of layers from one another. Diffraction models accounting for bending or isolation of chain layers in an oblique layer both explain the observed near invariance of certain intensities which are due to the coherent scattering from the line grating formed by rows of carbon atoms in the tilted chain aggregate. Forbidden reflections predicted by a bending model are less important than those anticipated by the multiple scattering from a laminated layer model. As these forbidden reflections are mostly identified for multilayer crystals and since crystal structure analysis indicates most of the long chain in a oblique monolayer to be diffracting coherently, the concentration of Reneker-type defects in the centers of chains is probably not great enough to isolate small chain length laminae within a monolayer.

Introduction

Owing to the difficulty of preparing single crystals of many long polymethylene chain compounds of size suitable for an X-ray crystal structure analysis, recent attention has been focused on the quantitative use of electron diffraction intensity data from more readily available thin microcrystals. The success of this endeavor has been less than consummate. Although the close correlation of single crystal electron diffraction data to earlier published texture data [1] has been established for orthorhombic paraffins [2], the naive use of kinematical diffraction theory necessarily must yield to a consideration of n-beam dynamical effects — even for monomolecular layers [2, 3]. However, a kinematical procedure may succeed in *ab initio* phase determination [4].

Another difficulty which may be more serious than the presence of dynamical effects, is the fact that the electron scattering from these crystals very often appears to be from the methylene subcell alone — irrespective of the polar group on the long chain. This is readily verified by an examination of published electron diffraction data. For example, diffraction intensities from compounds with a hexagonal methylene subcell have been found to be identical whether they be fatty acid, diglyceride or one of several phospholipids [2, 5–10]. Intensities from compounds packing in the orthorhombic perpendicular ($O_\perp$) methylene subcell are likewise identical for ketonic wax, paraffin, simple wax, and phospholipid [2, 10–12].

In our first attempt to characterize quantitatively the electron diffraction from these materials [2], it was also noted that multilayer crystals give diffraction intensities as if each layer were scattering independently from the others. This was tentatively interpreted in terms of bending of crystal layers by us [13] and as an eclipsing of chain axes in multilamellar crystals by other workers [14–17].

The purpose of this paper is to extend the understanding of electron diffraction from microcrystalline paraffinic derivatives by examination of the influence of "mosaic" distortions on the diffraction intensities. Thus, the first part will give a description of such crystal distortions by the use

Reprint requests to Dr. Douglas L. Dorset, Molecular Biophysics Department, Medical Foundation of Buffalo, Inc., 73 High Street, Buffalo, New York 14203, U.S.A.

of images obtained either by diffraction contrast or from metal-shadowed specimens. The second part will correlate the characterized crystal distortions to observed diffraction for several types of chain packing. For our analysis we shall keep in mind mainly two possible packing distortions which can affect the diffracted intensities from these thin crystals. Although they will be described in detail in the second part they are: (a) elastic bends as described by Cowley [18], and (b) paracrystalline disorders such as chain kinking, translations along chain axes and end plane misfits that would isolate crystallite layers [19—21].

Materials and Methods

a) Sample Preparation

Samples of the compounds in Table 1 were crystallized on carbon or Formvar-carbon covered 400 mesh copper electron microscope grids by rapid evaporation of a dilute solution in the indicated solvent. Diffraction spacings were calibrated with a gold powder standard evaporated onto a grid also containing the sample under study. Gold was also used to shadow crystals for study of morphology at low magnifications. Samples for reflection electron diffraction were evaporated onto a polished brass stud.

Table 1.

Compound	Source	Solvent
n-hexacosane (monoclinic)	Eastman Chemical Co., Rochester, New York	toluene
n-hexatriacontane (orthorhombic)	Aldrich Chemical Co., Milwaukee, Wisconsin	light petroleum
stearic acid, form B	Sigma Chemical Co., St. Louis, Missouri	ethanol
behenic acid, form B		ethanol or light petroleum
cetyl plamitate		ethanol or light petroleum
sn-glycero phosphoryl ethanolamine 1,2-dihexadecyl ether	Serdary Research Labs, London, Ontario, Canada	ethanol or light petroleum

b) Electron Diffraction and Microscopy

Several microscopes were used to obtain transmission diffraction and image data: Philips EM-300 equipped with $\pm 60°$ tilt, 360° rotation goniometer stage, Siemens IA, JEOL JEM-100C equipped with $\pm 60°$ tilt, 360° rotation goniometer stage, JEOL JEM-100U equipped with 30° tilt, 360° rotation tilt stage. Most work was done at 100 kV. For selective area diffraction, the effective areas were between 5 μ and 16 μ diameter. Most diffraction contrast work was carried out on the JEM-100U at low magnifications (2.5 k or 5.0 k). The incident beam or desired diffraction beam was isolated using the objective aperture for diffraction contrast images.

Radiation damage was minimized by using illumination conditions described before [2], i.e. maximal excitation of both condensors and insertion of a 20 μ aperture at condensor 2. Kodak screenless X-ray film was used to record both diffraction patterns and images. Typical recording times are 2 sec for diffraction patterns, 4 sec for bright field images, and 20 sec for dark field images.

Reflection diffraction experiments were performed at 50 kV on a Hitachi HU11 electron microscope equipped with a "high resolution electron diffraction holder" mounted below all the magnetic lenses. Exposures were recorded on electron image plates.

Diffraction intensities were obtained from diffraction films by scanning the patterns with a Joyce-Loebl Mk III flat bed microdensitometer and integrating under the peaks. The same philosophy for data reduction as used before was applied here [2].

c) Computations

Kinematical structure factor calculations for whole molecules were carried out using the program LINUS [22] on a CDC 6400 computer. For smaller chain segments they were calculated with a Hewlett-Packard HP 55 pocket calculator. Hydrogen atom contributions were ignored for the long chain molecules since, for covalent structures, the fractional electron scattering factor contribution is about the same as the X-ray values in comparison to the carbon scattering curve. Moreover, because of large librational motions of long carbon chains [23], the hydrogen atom temperature factors are large and are expected not to appreciably affect the accuracy of a phasing model based only on carbon atoms. An appreciation of the importance of hydrogen atoms to the refinement of these long chain structures can be gained from a classic paper by Jensen and Mabis [24]. Scattering factor tables were from Doyle and Turner [25].

Patterson maps for chain segments were formed by a graphical autocorrelation procedure found in many crystallographic textbooks [26].

Part I

Description of Crystal Deformations

In the following discussion, two types of chain packing will be considered, both of which include the $O_\perp$ methylene subcell. This subcell was first described by Müller [27] and has edges $a_s = 7.5$, $b_s = 5.0$, $c_s = 2.5$ Å. Type I is a class of compounds which pack with chain axes normal to the {001} surface of the crystal such that the incident beam is parallel to the c_s-axis of the subcell (for untilted crystals). Single layers of this chain packing are termed "rectangular" [28]. Of the compounds listed in Table 1, the orthorhombic polymorphs of n-hexatriacontane [29] and of cetyl palmitate [12] are represented. Crystals of this type have a characteristic {110} interfacial angle of 67° [30].

Type II compounds pack with the chain axes rotated about the subcell $a_s = 7.5$ Å axis by about 27°. Thus, the chain axes are inclined to the {001} face of the crystals by 63°. Kitaigorodskii [28] terms single layers as "oblique". A representation of this chain packing is shown in Figure 1. Compounds which pack this way include the monoclinic form of even paraffins [31], the B-form of fatty acids [32] and the monoclinic form of cetyl palmitate [12, 33]. Crystals of this type also have a characteristic {110} interfacial angle of 74° [34]. The (001) unit cell spacings are $a \simeq 5.6$ Å, $b \simeq 7.5$ Å.

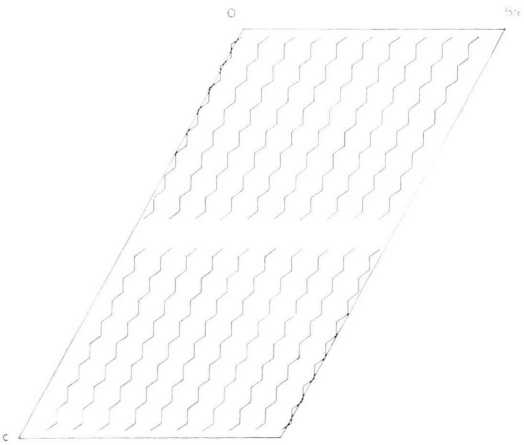

Fig. 1. Molecular packing of monoclinic n-hexatriacontane (010) projection (after Ref. [31]). For untilted crystals with oblique layers, incident beam is normal to the methyl end plane (see also Ref. [48]).

Type I. Crystals with Rectangular Layers

a) Elastic Bending

A clear example of elastic bending is shown by extinction lines in the bright field image of a n-hexatriacontane monolayer crystal ($t = 47$ Å) in Figure 2. Similar extinction contours have also been seen for microcrystals of this compound by Keller [35] but, due to the greater intensity of the incident electron beam in his earlier experiment, they were unstable. That these can be indexed according to strongly diffracting beams is evidenced in the sequence of bright field and dark field micrographs in Fig. 3 for a less uniformly bent n-hexatriacontane crystal than shown in Figure 2. (A representative diffraction pattern from this zone is shown in Fig. 7 or in an earlier paper [2].)

If we assume the kinematical theory to be approximately true, then we can use the spacing of the bend contours to estimate the amount of crystal bending. For two adjacent dark lines of a bend contour (bright field image) the difference in

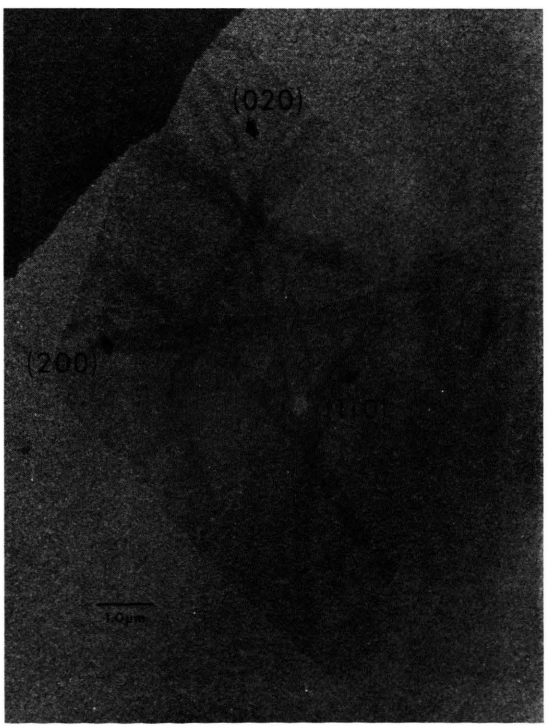

Fig. 2. Bright field diffraction contrast image of orthorhombic monolayer n-hexatriacontane ($t = 47$ Å) showing (indexed) bend contours due to (200), (110) and (020) beams.

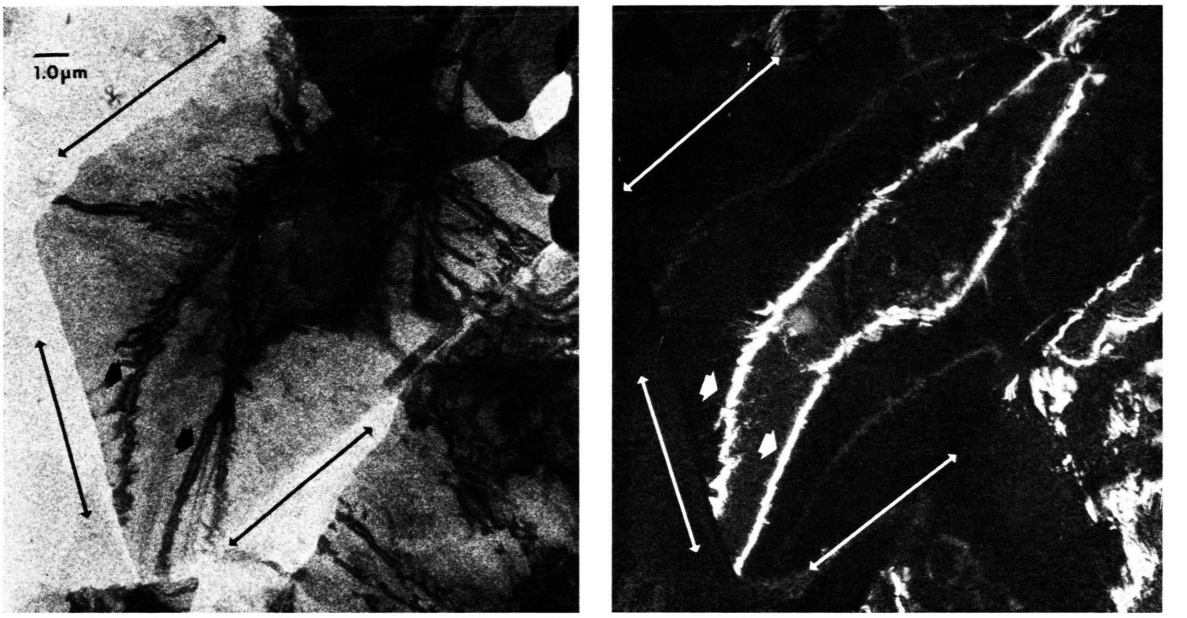

Fig. 3. Diffraction contrast images of n-hexatriacontane orthorhombic monolayer crystal. (a) Bright field image, (b) (110) dark field image. Corresponding crystal boundaries for diffraction contrast images are paralleled by double headed arrows. Bold arrows indicate bend contours due to (110) in both (a) and (b).

angle of incidence for the corresponding two Friedel-related reflections hkl is $2 \sin \theta_{hkl}$. Using $\Delta\theta \simeq 2 \sin \theta_{hkl}$, the spacing between the contour lines s, and the equation for an arc $R = s/\Delta\theta$, one can calculate the radius of curvature R for the crystal. The *amount* of bending in degrees which will be used for calculations in Part II includes the arc length between sets of bend contours due to the same reflections. Note in Fig. 2 that two sets of contours exist each for the Friedel pairs (110, $\bar{1}\bar{1}0$) and ($\bar{1}10$, $1\bar{1}0$). Using this criterion, the measured bends for monolayer orthorhombic n-hexatriacontane crystals are as much as 7.0° (±3.5°).

b) Crystal Surface Corrugation Due to Translation Along Chain Axes

Striations due to unit translations along chain axes were first seen by Keller [35] for heated orthorhombic n-hexatriacontane crystals. They have been shown to be parallel to either [100], [010] or [110]. Shadowed crystals demonstrate that the resultant "roofs" are methyl terminal faces with small subcell indices, e.g. $(201)_s$, $(101)_s$, $(102)_s$ etc., caused by integral shifts of $c_s = 2.54$ Å along the chain axis. Similar experiments were carried out for smaller alkanes and polyethylene [36, 37].

The formation of thin n-hexatriacontane microcrystals from warm solvent has often revealed corrugations and also gently undulated surfaces. For example, the multilayered crystal of Fig. 4 shows the presence of "b-line striations" (i.e. striations parallel to the b-axis), which is the highest temperature form before melting [35]. Orthorhombic cetyl palmitate crystals grown from hot ethanol (near the melting point of the wax) have marked corrugations (Figure 5). Here, the crystal habit is less well defined than for the paraffin.

c) Crystal Dislocations

The most obvious dislocation seen in metal-shadowed multilayer crystals of orthorhombic paraffins is the screw dislocation normal to {001}. This has been shown before for n-hexatriacontane [2] and explained very well with better specimens [38, 39]. Since the Burgers' vector for this dislocation is parallel to the incident beam, it will have no effect on the $hk0$ diffraction pattern.

Other dislocations are viewed by diffraction contrast electron microscopy in analogy to the studies on polyethylene [40—45]. An example of an *intra*lamellar edge dislocation [46] is seen in the indicated rotation moiré pattern of Figure 4c. As is discussed by White [45], gentle undulations in

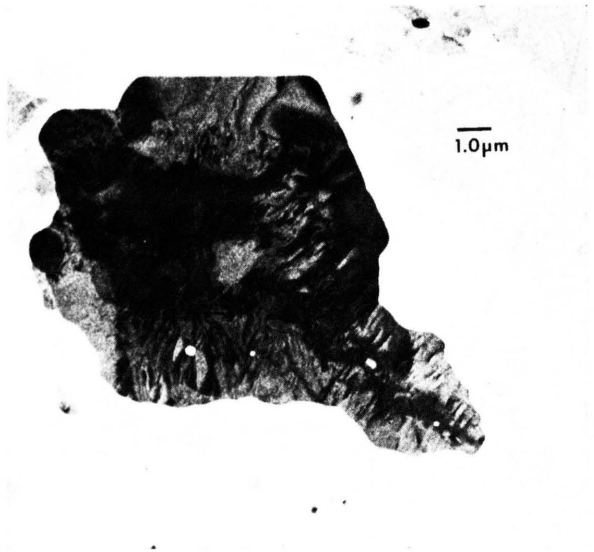

(a)

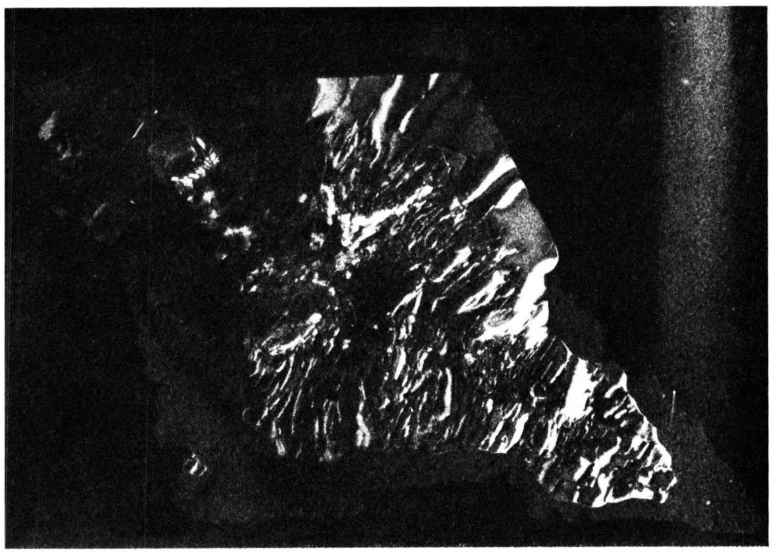

(b)

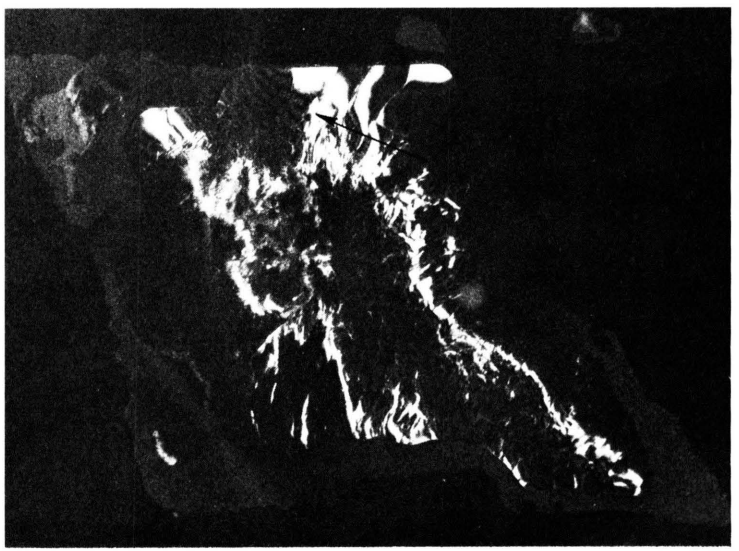

(c)

Fig. 4. Diffraction contrast of orthorhombic n-hexatriacontane multilayer. (a) Bright field image — note "b-lines" as seen by Keller [35], (b) (200) dark field image, (c) (110) dark field image — note moiré pattern with magnified representation of intralamellar edge dislocation.

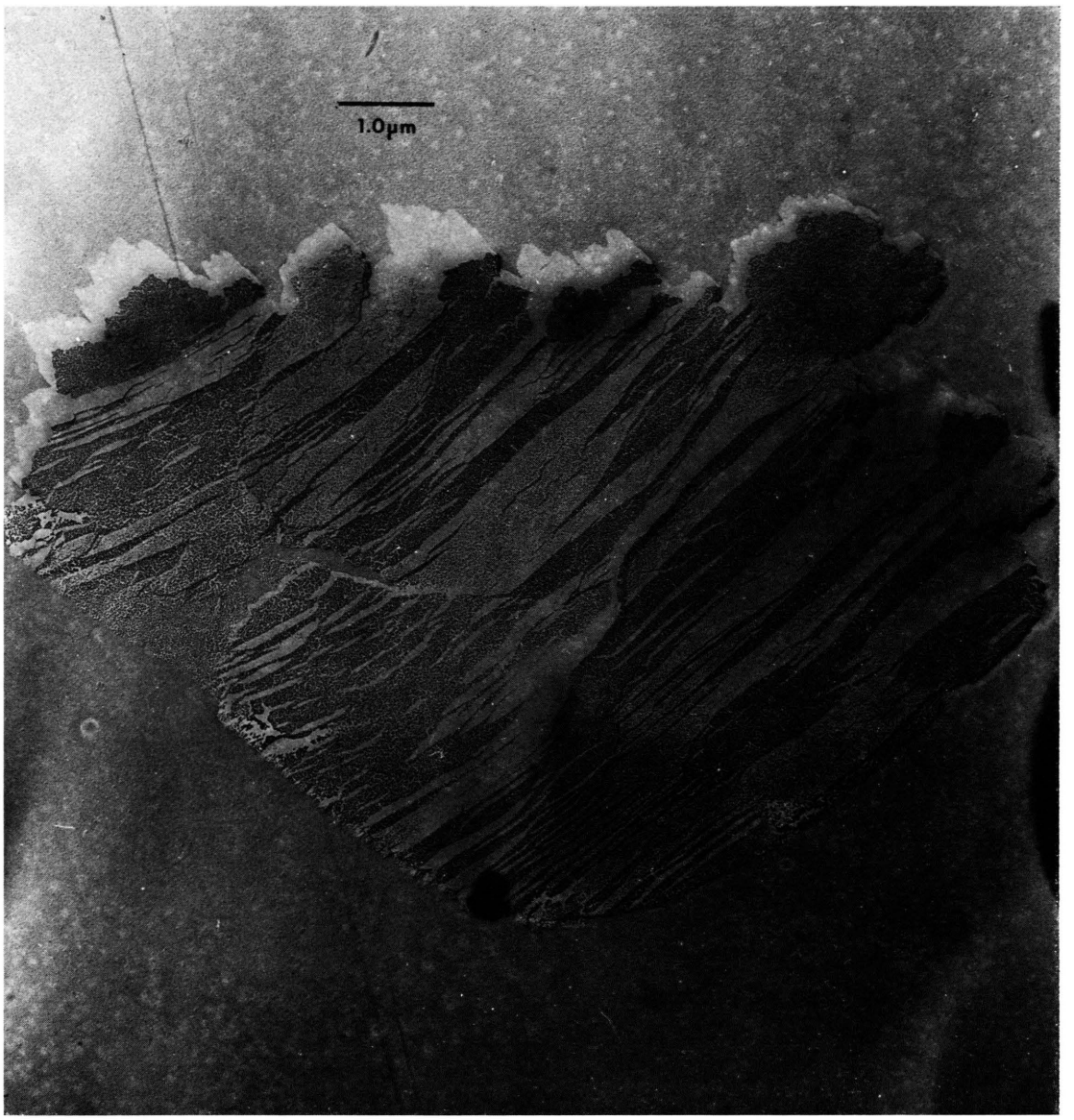

Fig. 5. Gold-shadowed crystal of orthorhombic cetyl palmitate showing corrugations due to chain translation along c_S.

the layer surfaces (evidenced by bend contours, *vide supra*) restrict the formation of moiré images to specific optimal regions on the crystal — i.e. only where the dark field image would be bright in the absence of other crystals. In other words, adjacent crystal layers must be mutually in correct position in order that diffraction interference may occur between them. Apparently this condition is less commonly satisfied for these crystals than for polyethylene. Indeed, the independence of contiguous layers may be indicated also by the absence of observed *inter*lamellar defects in our diffraction contrast experiments of the type described for polyethylene [42, 43, 47].

Type II. Crystals with Oblique Layers

a) Elastic Bending

Bend contours have also been observed in diffraction contrast images of B-form fatty acid

crystals and monoclinic crystals of cetyl palmitate. For untilted crystals there is one obvious set of bend contours (Fig. 6) due to the strongly diffracting (020) reflection of the monoclinic unit cell [48], which is also the (200) reflection of the subcell (using the axis assignments above). When such crystals are tilted about the 7.5 Å axis by 27°, the electron beam is parallel to the chain axes and the $O_{\perp}$ subcell $hk0$ diffraction patterns is again seen [12, 48]. Diffraction contrast micrographs of these tilted crystals are again similar to the untilted orthorhombic n-paraffin crystal (Figure 7).

Estimates of crystal bend from measured contour spacings are as large as 10° (±5.0°) for monolayer monoclinic cetyl palmitate crystals.

b) Surface Corrugation

In accordance with Keller's [35] experiments on monoclinic paraffin crystals, there have never been any observations of marked surface corrugations due to chain translations in crystals with oblique layers. Gentle surface undulations sometimes have been indicated in the diffraction contrast micrographs, however.

c) Crystal Dislocations

The screw dislocation normal to the crystal surface is often seen in metal-shadowed crystals of the fatty acids and cetyl palmitate. This has been dealt with in depth by Verma [49] and by Amelinckx [30]. Evidence of the polytypic crystal growth seen for fatty acids is also found for cetyl palmitate on the occasional observation of crystals with blunted tips in the direction of the long crystal diagonal [50] and also by the branching angle of an epitaxial dendritic form [51].

Part II

Electron Diffraction Intensities from Crystalline Long Chain Compounds

I. Characteristics of the Electron Diffraction Patterns

Before analysis of the diffraction from thin crystals of polymethylene compounds, it is beneficial to itemize several salient peculiarities which demand explanation:

a) Crystals with Rectangular Layers

1. Multilayer crystals of this type often give diffraction patterns with intensity distribution indicative of coherent scattering from individual layers only. This was noted in an earlier paper [2] on the electron diffraction from orthorhombic n-hexatriacontane where the diffraction was seen *not* to arise from the true unit cell (of two layers) found in the earlier X-ray structure determination [29]. It has also been noted for compounds packing in the "hexagonal" methylene subcell (see Introduction for references) which also forms rectangular layers.

2. For compounds with polar "functional" groups, it is often found that no contribution of these moieties is seen in the diffraction intensity distribution. Appropriate references to this are given in the Introduction.

b) Crystals with Oblique Layers

1. For untilted crystals of this type, a variety of diffraction patterns with the same spacings but different intensity distributions can be seen. The salient common feature amongst them are the layer line relative intensities at $h=0$ and $h=5$. (We are using the monoclinic unit cell notation with $a \cong 5.6$ Å, $b \cong 7.5$ Å; also, see Fig. 1 of Ref. [3] for representative diffraction pattern of this zone.) A preliminary effort to interpret some of the other layer line intensity variations was made on the basis of n-beam dynamical theory [12] but the explanation was inadequate.

2. Tilting these oblique layer crystals by 27° about the 7.5 Å axis gives the expected (001) projection of the subcell. The $hk0$ intensities agree very well with the phasing model and there is *no* variaton in the pattern from crystal to crystal except for more or less contribution of multiple scattering, seen also for orthorhombic paraffins [12,48].

3. Using the diffraction patterns from appropriately tilted crystals, no contribution from polar groups is found in the intensity distribution; there is only diffraction from the methylene subcell. Another indication of this from untilted crystals is given in Table 2 which lists $0k0$ and $5k0$ observed structure factors for several isostructural compounds with different polar groups.

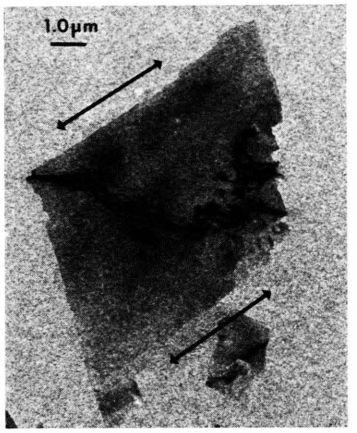

6 (a)

6 (b)

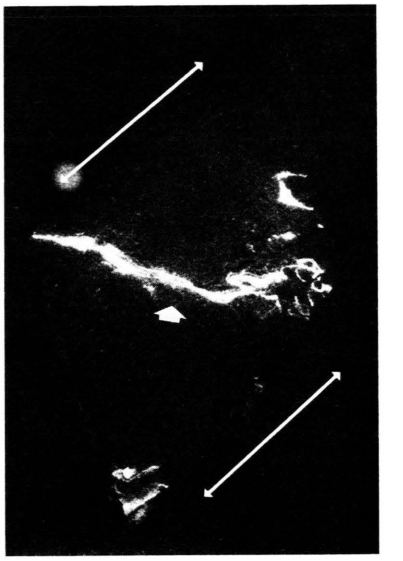

Fig. 6. Monoclinic B-form behenic acid crystal — untilted (a) bright field image showing bend contour, (b) (020) dark field image. Corresponding crystal boundaries are paralleled by double headed arrows. Positions of the (020) bend contours are indicated by bold arrows in (a) and (b).

7 (a)

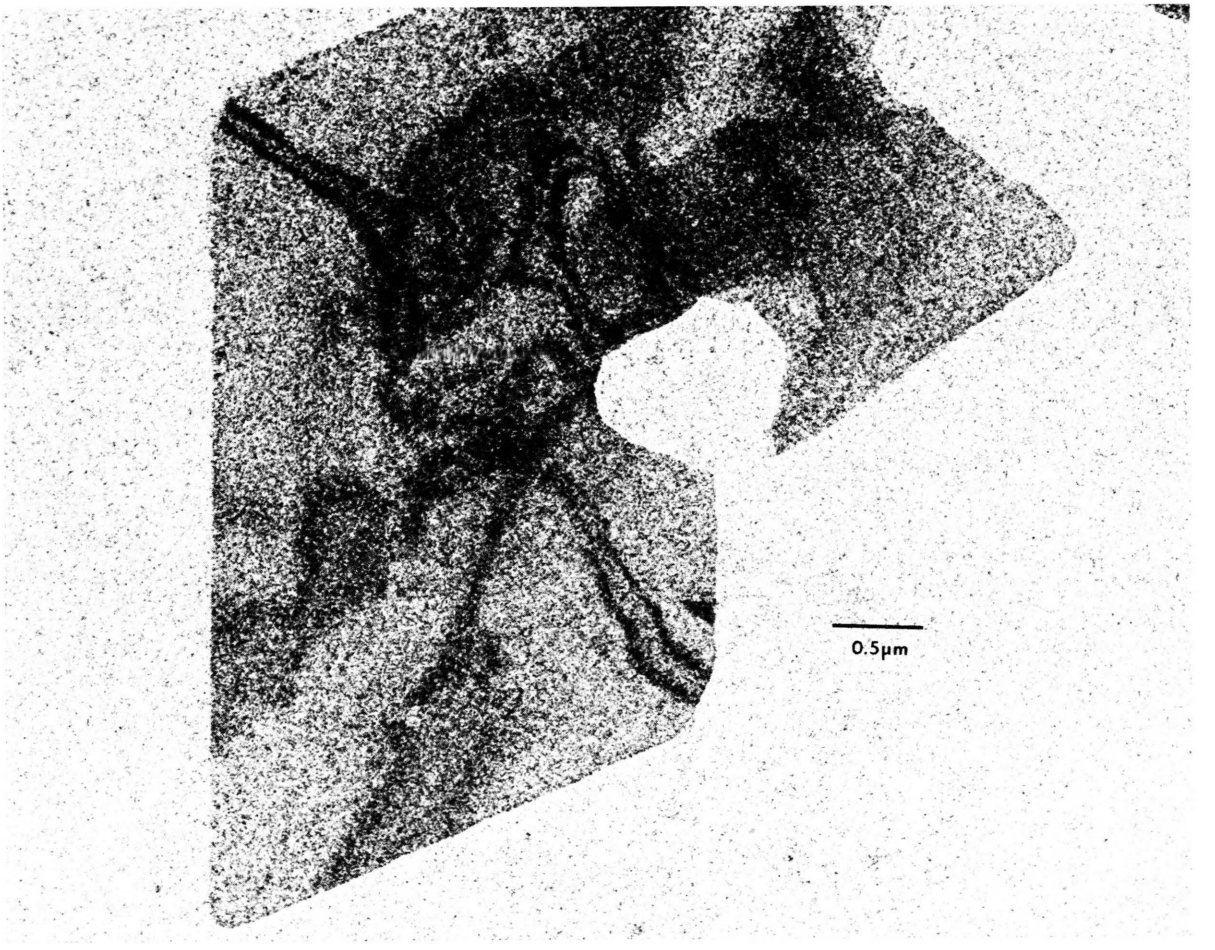

7 (b)

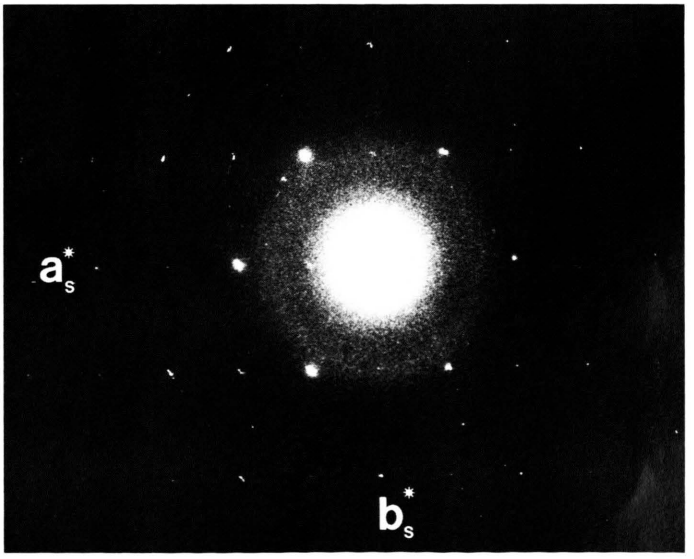

7 (c)

◀

Fig. 7. Diffraction contrast images from B-form behenic acid crystal tilted 30° about b^* axis. (a) Bright field image showing bend contours, (b) $(110)_S$ dark field image, (c) $(hk0)_S$ diffraction pattern.

Table 2. Comparison of representative electron diffraction data from six isostructural long chain compounds with kinematical structure factors for layer lines $h = 0$, $h = 5$ at $B = 0.0$ Å^2. Residual $R = (\Sigma||F_o| - |k|F_c||)/\Sigma|F_o|$.

Compound	Orthorhombic n-hexatriacontane 30° tilt ~ a	Monoclinic n-hexacosane	Stearic acid form B	Behenic acid form B	Cetyl palmitate	sn-Glycerophosphoryl ethanolamine, 1,2-dihexadecyl ether
$h\,k$	$\|F_o\|$	$\|F_o\|$	$\|F_o\|$	$\|F_o\|$	$\|F_o\|$	$\|F_o\|$
02	5.92	5.95	6.16	5.79	5.44	5.10
04	2.71	3.08	3.04	2.62	2.56	2.59
06	1.19	1.00	0.89	0.97	0.94	0.90
51	1.73	1.44	2.08	1.93	2.20	2.55
52	0.0	0.0	0.0	0.0	0.0	0.0
53	0.98	0.97	0.83	1.38	1.18	1.23
54	0.0	0.0	0.0	0.0	0.0	0.0
55	0.52	0.50	—	0.50	0.88	0.84
R	0.18	0.22	0.16	0.14	0.21	0.25

II. Possible Diffraction Models

a) Diffraction from Elastically Bent Crystals

Since there are obvious bends in the crystals of these long chain materials, a cogent model for the diffraction is thought to be that proposed by Cowley [18]. Given an elastically bent crystal, Cowley describes the smearing of Patterson peaks by a Gaussian approximation for the arcing:

$$g(p/r_i) = \frac{\sigma}{r_i\sqrt{\pi}} \exp(-\sigma^2 p^2 r_i^{-2})$$

where p is the distance measured along the arc, r_i is the length of the Patterson vector and σ is a constant describing the amount of bending. Since p/r_i is clearly α, the angle of bending in radians, the limit of the arcing if considering the Gaussian half width is then $\sigma = \alpha^{-1}$. Since the intensity of a reflection $I(\boldsymbol{s})$ is the Fourier transform of the Patterson function,

$$I(\boldsymbol{s}) = \sum_i W_i(\boldsymbol{s}) \cdot \exp(2\pi i\, \boldsymbol{r}_i \cdot \boldsymbol{s}) \exp - \left[\frac{\pi^2}{\sigma^2} s^2 z_i^2\right] \quad (1)$$

describes how the diffracted intensity from a bent crystal is affected by this distortion. Here $W_i(\boldsymbol{s})$ is the Fourier transform of the Patterson peak $w_i(\boldsymbol{r})$, $\boldsymbol{s}$ is the reciprocal vector and s its magnitude. The length $z_i = r_i \cos\alpha$ describes the z component of the Patterson vector $\boldsymbol{r}_i$ for a bent crystal. From the z-component is derived an estimate of the coherent scattering thickness, $z_0 = \sigma/\pi s$, beyond which Patterson vectors are not anticipated to contribute appreciably to the intensity. Notice that this scattering thickness is dependent on $\sin\theta/\lambda$. The existence of such modulation of the diffraction patterns due to uniform bends has been verified for several nearly perfect paraffinic crystals [52].

The (001) projection of the zig-zag carbon chain for the oblique layers is shown in Figure 8. Initial model calculations were carried out with a four

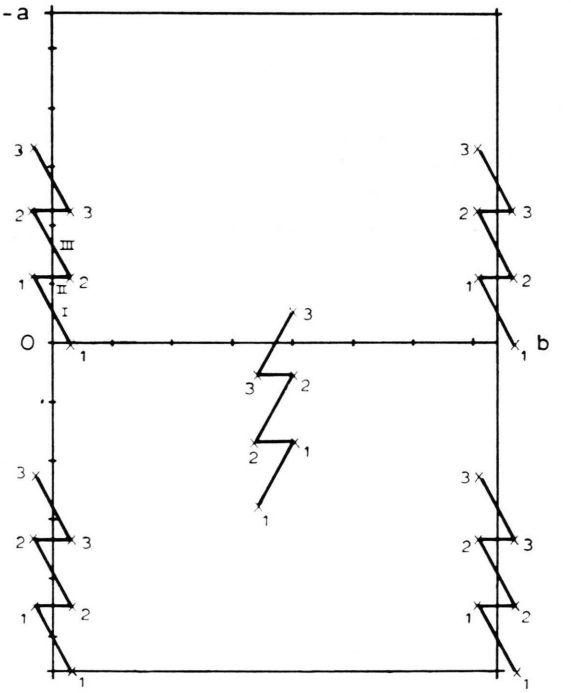

Fig. 8. Projection of oblique layer along [001]. For model calculations with small number of carbons (Section IIb), arabic numbers indicate order of inclusion. Roman numerals denote shifted apparent unit cell origin after addition. For Patterson map (Section IIa) a desired chain length was graphically autocorrelated.

carbon chain segment of this projection with requisite plane group symmetry pgg. The Patterson map of this segment is shown in Fig. 9 assuming no maximum vector length. If one assumes a maximum vector length of only two carbon atoms from any given carbon in a graphical autocorrelation process, then the Patterson function is truncated as shown in Figure 10. Thus the symmetry of the intensity distribution after Fourier transformation no longer satisfies systematic absences along b^* as demanded for space group pgg, while those along a^* are still satisfied.

Next, a more rigorous calculation was carried out for a linear sixteen carbon chain with this oblique packing scheme. Again, the Patterson function was found by the graphical autocorrelation process. The Fourier transform of the Patterson function formed from point atoms gives intensities which are squares of the normalized structure factors, E_{hkl}. The modulation of these intensities due to crystal bending, expressed by Eq. (1), is a summation of exponentials which are in effect, temperature factors. Thus, an altered intensity I' will be expressed as a summation of intensities I_i formed by transforming Patterson peaks representative of increasing z_i vector lengths i.e.

$$I' = \sum_i I_i \exp(-2 B_i \sin^2 \theta/\lambda^2)$$

where $I_i = W_i(s) \exp(2\pi i \boldsymbol{r} \cdot \boldsymbol{s})$ then from (1),

$$2 B_i \sin^2 \theta/\lambda^2 = (4\pi^2/\sigma^2) z_i^2 \sin^2 \theta/\lambda^2$$

or

$$2 B_i = (4\pi^2/\sigma^2) z_i^2 .$$

Again, a temperature factor B_i holds for a given Patterson vector with z_i and as z_i becomes large the effect of the apparent temperature factor does also.

Calculations of intensities for model $n\mathrm{C}_{16}$ chains in oblique crystals with increasing bending were effected from the Patterson function shown schematically in Table 3, without the assumption of zero weight beyond a z_0 value used by Cowley and Goswami [53] for more complex silicate structures (yet, it is instructive to examine the variation of z_0 with increasing reciprocal distance as

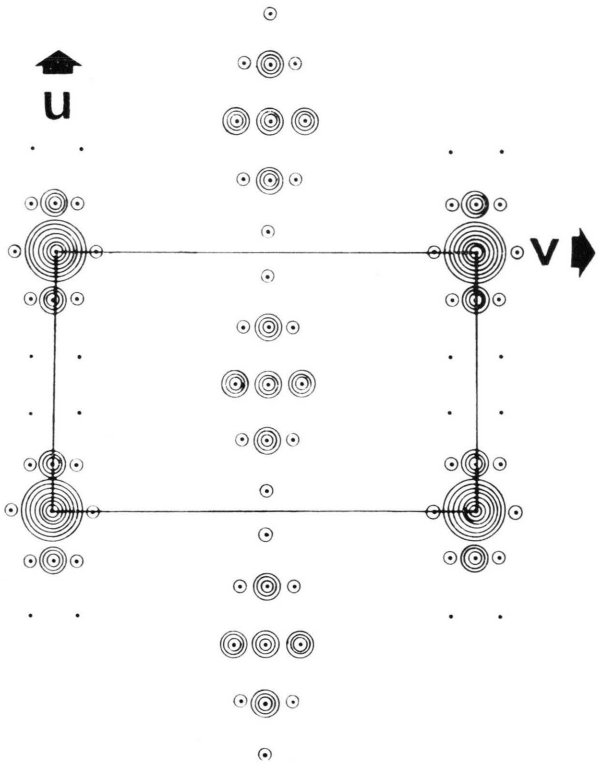

Fig. 9. Patterson map for oblique four carbon chain, zero layer. Peaks centered about the origin (0, 0) are due to the molecular self-image. Those centered about (1/2, 1/2) are due to inter-molecular vectors.

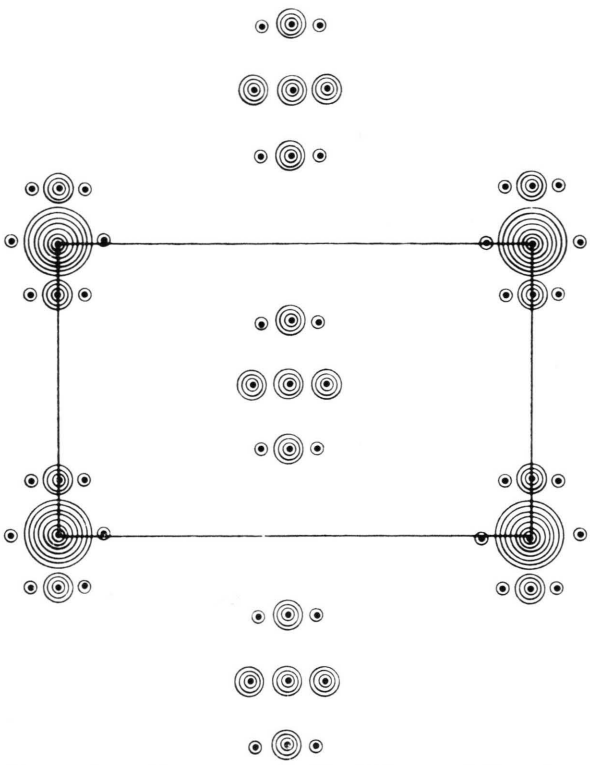

Fig. 10. Some Patterson as in Fig. 10 but resolution along z is restricted to two carbons in chain. Note elimination of peaks farthest from origin at (0, 0) or (1/2, 1/2).

Table 3. Patterson function terms for sixteen carbon chain of point atoms. The chain is tilted to form the oblique monoclinic paraffinic structure.

Corner of map				Center of map		
1	0	1	$\overline{1}$	0	2	0
2	4	2	0.20a	2	4	2
4	8	4		4	8	4
6	12	6		6	12	6
8	16	8		8	16	8
10	20	10		10	20	10
12	24	12	u	12	24	12
14	28	14		14	28	14
14	32	14	v	16	28	16
14	28	14		14	28	14
12	24	12		12	24	12
10	20	10		10	20	10
8	16	8		8	16	8
6	12	6		6	12	6
4	8	4		4	8	4
2	4	2		2	4	2
1	0	1		0	2	0

0.076b

number "32" at coords (0, 0)

middle number "28" at coords (1/2, 1/2)

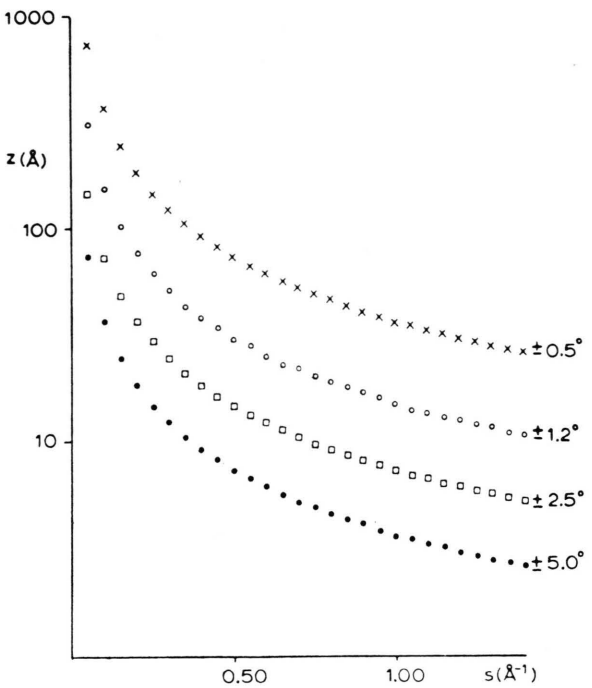

Fig. 11. Predicted maximum Patterson vector length along z for given crystal bends as a function of $s = d^*$.

shown in Figure 11). The normalized structure factors from these calculations are given in Table 4, scaled to a constant value of ($|E_{020}| + |E_{040}| + |E_{060}| + |E_{510}| + |E_{530}| + |E_{550}|$). The scaling represents a normalization to constant intensity for the most intense layer lines in the diffraction pattern. These layer lines represents the major diffraction bands from a line grating structure formed from rows of carbon atoms in this (001) projection (see Figure 8).

Table 4. Normalized structure factor magnitudes for bent oblique layer crystals derived from Fourier transform of Patterson function of linear C_{16} chain. Scaling such that $|E_{020}| + |E_{040}| + |E_{060}| + |E_{510}| + E_{530}| + |E_{550}|$ is constant.

	$\lvert E_{hk0}\rvert$				
$hk0$	$\pm 0.0°$	$\pm 2.5°$	$\pm 5.0°$	$\pm 7.5°$	$\pm 10.0°$
01	0	0.54	1.20	1.85	2.39
02	56.88	66.71	75.21	78.95	80.72
03	0	3.59	5.61	6.48	7.31
04	37.04	39.74	39.98	39.65	39.45
05	0	6.20	7.89	9.19	10.37
06	9.05	8.74	8.12	8.09	7.99
10	0	0	0	0	0
11	10.78	12.71	14.38	14.84	22.18
12	3.49	3.77	4.00	3.20	3.61
13	7.90	8.55	12.50	22.87	32.08
14	6.21	5.91	6.91	8.06	9.09
15	3.27	3.64	9.82	14.73	17.35
16	7.54	6.85	8.44	9.79	11.04
20	1.50	3.71	3.21	4.39	6.51
21	1.13	1.52	1.99	2.32	2.62
22	1.33	1.63	3.10	4.68	8.91
23	3.07	4.39	5.56	6.48	7.31
24	2.19	2.43	3.24	6.41	12.48
25	4.36	6.37	7.89	9.19	10.37
26	0.40	0.55	1.44	3.02	4.67
30	0	0	0	0	0
31	3.73	4.16	5.17	7.83	15.73
32	2.15	3.10	3.88	4.53	5.11
33	1.20	1.75	3.64	8.88	17.25
34	3.84	5.58	6.91	8.06	9.09
35	0.54	0.91	2.55	6.92	11.46
36	4.65	6.81	8.39	9.79	11.04
40	10.48	11.48	27.97	40.75	47.46
41	1.79	1.64	1.99	2.32	2.62
42	13.45	10.59	26.22	36.77	42.05
43	5.00	4.54	5.56	6.48	7.31
44	6.39	8.15	18.93	24.38	26.93
45	7.08	6.41	7.89	9.19	10.37
50	0	0	0	0	0
51	62.22	57.87	54.33	52.79	52.05
52	0	3.15	3.88	4.53	5.11
53	48.32	43.70	40.70	39.48	38.94
54	0	5.61	6.91	8.06	9.09
55	23.52	20.27	18.69	18.07	17.88

A plot of summed layer line structure factors for constant h is given in Fig. 12 for the various crystal bends considered. None of the layer line scattering amplitudes remain constant with crystal bending. However, the layer line at $h = 0{,}5$ are found to change least. The scattering amplitudes at other lines change dramatically relative to these when the oblique layer crystal is bent.

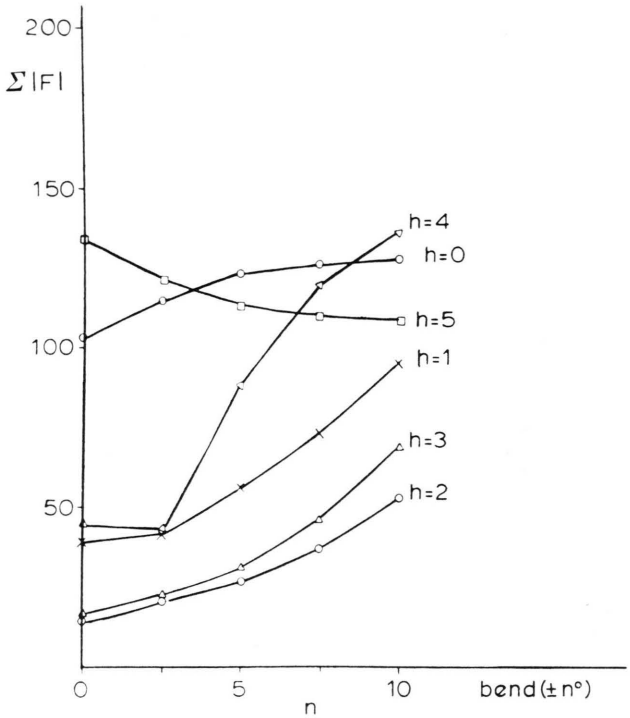

Fig. 12. Summed $hk0$ structure factor magnitudes $0 \leqq k \leqq 6$ for layer lines of constant h plotted against increasing crystal bend. For $h = 0, 5$, weak forbidden F's not used in summation.

b) Independently Scattering Layers of Arbitrary Thickness

Another model, suggested by observations of undulated surfaces in diffraction contrast micro graphs of multilayered crystals, is a mosaic model which assumes a laminate of independently scattering layers in a stack [54]. Its effects are independent of $\sin\theta/\lambda$. A previous paper estimated $hk0$ diffraction patterns of orthorhombic paraffin to be free of multiple scattering for thicknesses less than five layers. This guess was arrived at after an assay of shadowed crystals on a grid used for diffraction experiments [2]. Further work in which diffraction contrast images were recorded after the $hk0$ diffraction pattern shows that, for n-hexatriacontane, multiple scattering can arise from bilayer crystals. Again, the intensity distribution is still that of the monolayer and not the unit cell found by Teare [29]. The assumption of independent scattering layers has been used to explain the formation of moiré images of polyethylene by diffraction contrast [40].

Examination of Fig. 8, which is the (001) projection of an oblique layer relevant to this discussion, indicates that the major constant contributor to the $hk0$ diffraction pattern should be the interference function due to rows of carbon atoms. These would account for invariant relative intensities of reflections in layer lines $h = 0$ and $h = 5$ in this model (see Fig. 1 of Ref. [3]). The intensities of other layer lines relative to these two are dependent on the *number* of carbons in the chain as is shown in Table 5 and Figure 13. The carbon coordinates used for the model calculations are given in Table 6. If the presence of Reneker type [21, 55] point defects can be assumed, then a paraffinic monolayer also could be imagined to be composed of a stack of independent layers. In any case, the restriction of a number of layers does not cause violation of pgg symmetry *per se*. However, forbidden reflections would arise from multiple scattering.

III. Intensity Data

In order to test these models on crystals with oblique layers, several $hk0$ diffraction patterns from the B-form of stearic and behenic acid were examined for overall similarities. Scaling a group

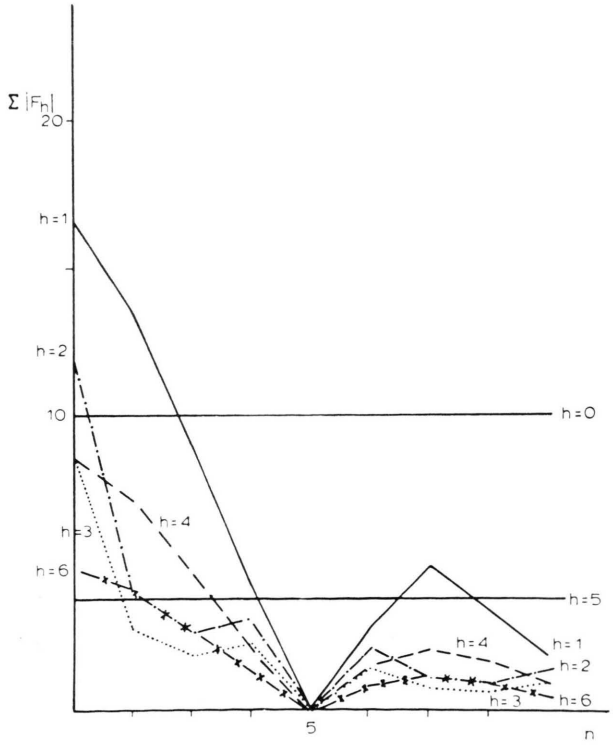

Fig. 13. Summed $hk0$ structure factor magnitudes, $0 \leqq k \leqq 8$ for layer lines of constant h plotted against the number of coherently scattering carbon pairs n in a layer. See Table V.

Table 5. $hk0$ kinematical structure factors calculated for successive carbon pairs using transformed monoclinic n-hexatriacontane (001) coordinates ($B = 0.0$ Å^2).

	Number of pairs								
$h\,k$	1	2	3	4	5	6	7	8	9
02	6.75	6.75	6.75	6.75	6.75	6.75	6.75	6.75	6.75
04	2.47	2.47	2.47	2.47	2.47	2.47	2.47	2.47	2.47
06	0.33	0.33	0.33	0.33	0.33	0.33	0.33	0.33	0.33
11	6.48	5.24	3.49	1.62	0.00	− 1.08	− 1.50	− 1.31	− 0.72
12	1.85	1.50	1.00	0.46	0.00	− 0.31	− 0.43	− 0.37	− 0.21
13	3.25	2.63	1.75	0.81	0.00	− 0.54	− 0.75	− 0.66	− 0.36
14	1.92	1.55	1.03	0.48	0.00	− 0.32	− 0.44	− 0.39	− 0.21
15	0.89	0.73	0.48	0.22	0.00	− 0.15	− 0.21	− 0.18	− 0.10
16	1.33	1.08	0.72	0.33	0.00	− 0.22	− 0.31	− 0.27	− 0.15
20	1.97	0.61	− 0.40	− 0.49	0.00	0.33	0.17	− 0.15	− 0.22
21	1.36	0.42	− 0.28	− 0.34	0.00	0.23	0.12	− 0.11	− 0.15
22	1.44	0.45	− 0.30	− 0.36	0.00	0.24	0.13	− 0.11	− 0.16
23	2.67	0.83	− 0.55	− 0.67	0.00	0.45	0.24	− 0.21	− 0.30
24	0.60	0.19	− 0.12	− 0.15	0.00	0.10	0.05	− 0.05	− 0.07
25	2.30	0.71	− 0.47	− 0.58	0.00	0.38	0.20	− 0.18	− 0.26
26	0.09	0.03	− 0.02	− 0.02	0.00	0.02	0.01	− 0.01	− 0.01
31	− 1.24	0.38	0.25	− 0.31	0.00	0.21	− 0.11	− 0.10	0.14
32	1.63	− 0.51	− 0.34	0.41	0.00	− 0.27	0.14	0.13	− 0.18
33	− 0.74	0.23	0.15	− 0.19	0.00	0.12	− 0.07	− 0.06	0.08
34	2.05	− 0.64	− 0.42	0.51	0.00	− 0.34	0.18	0.16	− 0.23
35	− 0.24	0.08	0.05	− 0.06	0.00	0.04	− 0.02	− 0.02	0.03
36	1.62	− 0.50	− 0.33	0.41	0.00	− 0.27	0.14	0.13	− 0.18
40	− 2.33	1.89	− 1.26	0.58	0.00	− 0.39	0.54	− 0.47	0.26
41	0.39	− 0.32	0.21	− 0.10	0.00	0.07	− 0.09	0.08	− 0.04
42	− 1.87	1.51	− 1.01	0.47	0.00	− 0.31	0.43	− 0.38	0.21
43	0.90	− 0.73	0.48	− 0.23	0.00	0.15	− 0.21	0.18	− 0.10
44	− 0.94	0.76	− 0.50	0.24	0.00	− 0.16	0.22	− 0.19	0.10
45	0.92	− 0.75	0.50	− 0.23	0.00	0.15	− 0.21	0.19	− 0.10
46	− 0.16	0.13	− 0.09	0.04	0.00	− 0.03	0.04	− 0.03	0.02
51	− 1.91	1.91	− 1.91	1.91	− 1.91	1.91	− 1.91	1.91	− 1.91
52	0.00	0.00	0.00	0.00	0.00	0.00	0.00	0.00	0.00
53	− 1.27	1.27	− 1.27	1.27	− 1.27	1.27	− 1.27	1.27	− 1.27
54	0.00	0.00	0.00	0.00	0.00	0.00	0.00	0.00	0.00
55	− 0.49	0.49	− 0.49	0.49	− 0.49	0.49	− 0.49	0.49	− 0.49
56	0.00	0.00	0.00	0.00	0.00	0.00	0.00	0.00	0.00
60	− 1.16	0.94	− 0.63	0.29	0.00	− 0.19	0.27	− 0.24	0.13
61	− 0.19	0.16	− 0.10	0.05	0.00	− 0.03	0.04	− 0.04	0.02
62	− 0.98	0.79	− 0.53	0.25	0.00	− 0.16	0.23	− 0.20	0.11
63	− 0.49	0.40	− 0.27	0.12	0.00	− 0.08	0.11	− 0.10	0.05
64	− 0.54	0.44	− 0.29	0.14	0.00	− 0.09	0.13	− 0.11	0.06
65	− 0.59	0.48	− 0.32	0.15	0.00	− 0.10	0.14	− 0.12	0.07
66	− 0.11	0.09	− 0.06	0.03	0.00	− 0.02	0.02	− 0.02	0.01

Table 6. Carbon atom coordinates (derived from Shearer and Vand [31], after transformation to $\beta = 91.67°$).

C 1	0.000	0.038	layer 1
C 2	− 0.200	− 0.038	
C 3	− 0.200	0.038	layer 2
C 4	− 0.400	− 0.038	
C 5	− 0.400	0.038	layer 3
C 6	− 0.600	− 0.038	
etc.			

of observed structure factors from the two layer lines to an arbitrary value:

$$|F_{040}| + |F_{510}| + |F_{530}| = 10,$$

and averaging over a group of different diffraction patterns gave values and standard deviations as listed in Table 7 for 30 behenic acid crystals and for 11 stearic acid crystals. (The value of $|F_{020}|$ was not included in the scaling in order to avoid spurious effects due to exceeding the linear response to the film for this intense reflection.) Using the same scaling parameters, averages were taken over all patterns for five reflections in layer lines $h = 1$. These are also shown in Table 7 and are seen to have standard deviations greater than for the reflections in layer lines $h = 0$ and $h = 5$.

Further tests were made on the isostructural monoclinic cetyl palmitate. Averages of observed

Table 7. Averaged structure factor values for fatty acid oblique layer crystals with standard deviations.

Stearic acid				Behenic acid			
$hk0$	$\langle F \rangle$	σ	error %	$hk0$	$\langle F \rangle$	σ	error %
020	12.68*	2.17	17	020	10.78*	1.32	12
040	5.20	0.60	12	040	5.25	0.59	11
060	1.89	0.47	25	060	1.89	0.44	23
510	2.86	0.43	15	510	3.03	0.46	15
530	1.92	0.28	15	530	1.72	0.28	16
110	3.57	1.67	47	110	2.00	1.09	55
120	1.74	0.41	24	120	1.79	0.49	29
130	1.81	0.53	28	130	1.72	0.92	52
140	0.97	0.38	39	140	1.06	0.43	41
150	1.20	0.61	50	150	1.07	0.43	40

* Average over films where linear response not exceeded, N = 7.

* Average over films where linear response not exceeded, $N = 21$.

structure factor values for layer lines $h = 0$ and $h = 5$ (scaling as before) are given in Table 8 with standard deviations. The average is over 48 separate diffraction patterns. A group of patterns for which diffraction contrast bright field micrographs of the crystals were also available were then examined and grouped according to origin from monolayer or multilayer crystal. The standard deviation of averaged $1k0$ reflections from monolayer crystals (eleven diffraction patterns) are shown in Table 8 to be comparable to those of the $0k0$ and $5k0$ reflections. Since the % error for layer line $h = 1$ is of the same order to magnitude found for layer lines $h = 0$ and 5, and since these collectively represent the major intensity in this zone, *the overall diffraction intensity from an oblique monolayer is nearly constant* just as is the overall intensity from a rectangular layer.

The claim of overall congruence for relative $hk0$ diffraction intensities cannot be made for multilayered crystals except for the two mentioned layer lines which bespeak the interference function for carbon rows. This is demonstrated also in Table 8 for diffraction patterns from multilayers, scaled as before. Unlike the monolayer case, the standard deviation of $|F_{1k0}|$ is much larger than that of $|F_{0k0}|$ or $|F_{5k0}|$.

IV. Analysis

Modulation of diffraction intensities by crystal bending has been demonstrated for nearly perfect paraffin crystals [52]. However, distinguishing bend effects from those of layering effects due to point defects and mismatch of end planes is difficult. Both models will account for the near invariance of the $0k0$ and $5k0$ intensities experimentally shown in Table 7 and 8 for oblique layers since the fluctuation of structure factor moduli of $h = 0{,}5$ for the bent model is probably within the measurement error. Also, both models will account for a variation of reflection intensities in layer lines where $h \neq 0{,}5$.

Experimental data for cetyl palmitate monolayers which have bends from 0.7° to 5.0° show that the *total* diffracted $hk0$ intensity is fairly constant. The average crystal bend is around 2.7° (±1.3°). Of the three intense $1k0$ reflections measured, only the (150) intensity would arise from coherent diffraction from less than a monolayer at this average bend, and this may account for the slightly higher % error seen in the mean value of this reflection. Consistent with general observation, average measured bends from multilayer crystals of cetyl palmitate are greater than found for monolayers and would account for the much greater variation of $1k0$ reflections. Moreover, the greater relative value of $4k0$ reflections predicted by the bend model is often observed in diffraction patterns from bent multilayers.

Table 8. Average structure factor values for oblique layer crystals of monoclinic cetyl palmitate with standard deviation.

All crystals $N = 48$				Monolayer crystals $N = 11$				Multilayer crystals $N = 8$			
$hk0$	$\langle F \rangle$	σ	error %	$hk0$	$\langle F \rangle$	σ	error %	$hk0$	$\langle F \rangle$	σ	error %
020	11.43*	1.77	15	110	1.46	0.22	15	110	1.98	0.88	44
040	5.46	0.42	8	120	0	—	—	120	0.62	0.14	23
060	2.15	0.36	17	130	1.23	0.20	16	130	1.15	0.38	33
510	2.80	0.31	11	140	0	—	—	140	0.64	0.21	33
530	1.74	0.28	16	150	0.83	0.20	24	150	0.66	0.17	25
550	0.99	0.17	17								

* Average over films where linear response not exceeded, $N = 18$.

Yet other data indicate independent scattering from separate layers in the crystal. For example, the strong forbidden reflections along the b^* axis predicted by a simple bend model for $hk0$ patterns from oblique layers are not seen in actual diffraction patterns from multilayer crystals. The strongest forbidden reflections lie along a^*, an effect which is predicted using the intensity self-convolution model of Cowley et al. [54], and is more consistent with a crystal composed of independent layers.

Another difficulty with the bend model is that it does not account for the absence of diffraction from polar regions of a long chain molecule. Patterson functions formed from such structures at limited z-resolution do not give greatly decreased contribution from the polar region. Negation of coherent scattering from polar groups could be explained in terms of point defects, a contention which is further supported by an X-ray crystal structure of an ω-brominated fatty acid anhydride [56] and a cholesterol ester [57], in which the terminal bromines are sometimes found in a *gauche* conformation with the rest of the acyl chain. Moreover, Reneker-type defects [21, 55] have been found in the crystal structure of cholesteryl oleate and prostaglandin $F_{2\alpha}$ [58, 59]. They have been proposed for polyethylene [55] and n-paraffins [60] and would account for the extreme broadening of $hk0$ reflections along c^*, as seen in rocking curve plots for n-hexatriacontane [2] and for behenic acid (Fig. 14).

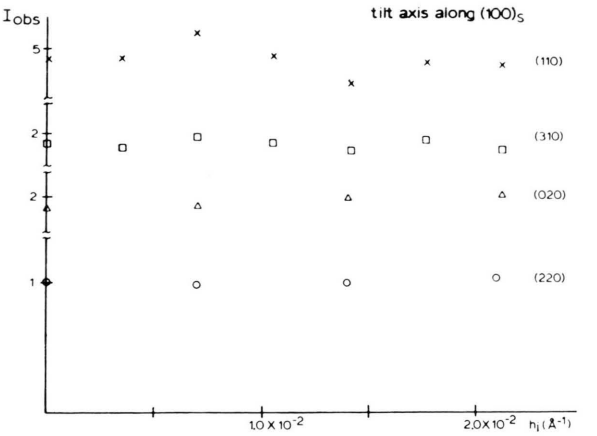

Fig. 14. Rocking curves for thin behenic acid, B-form, crystal tilted from 30° to 24° about b^* axis, showing smearing of shape transform due to crystal imperfections.

V. Random Translations Along the Chain Axes

Translations along the chain axes have no effect on the $hk0$ diffraction pattern from rectangular layers [61], whether they be random or integral. Such translations would affect oblique layer diffraction intensities from the chain only if they were random and non-integral values of $c_s = 2.5$ Å.

Reflection electron diffraction patterns were obtained from layers of n-hexatriacontane and behenic acid evaporated onto a polished brass stud from the solvent. The solutions were the same used for forming crystals for transmission diffraction studies. No effort was made to achieve a very flat metal surface. It is expected that similar conditions prevail in the sample formation as for preparation on e.m. grids. The strong subcell band at 1.3 Å in the reflection patterns in Fig. 15 thus indicates that the polymethylene chains, if translated, are shifted by integral values of c_s. The fatty acid crystals are expected to be multilamellar and do not exhibit the transformation to a soap obtained by forming a monolayer of the material rubbing on an active metal surface [62]. A single crystal pattern is often seen for the paraffin, and a polycrystalline pattern always found for the fatty acid, consistent with our observation of overall crystal size differences in transmission experiments. The chain tilt angle measured for the behenic acid pattern is the B-polymorph value of 27°.

Integral chain slips coupled with above mentioned bond rotations at the end groups would cause random disturbance in polar moiety packing such that they would not contribute to the diffracted intensity.

Crystal Structure Analysis

Cetyl palmitate has been optimal for studying the diffraction from monolayer crystals because of the large surface area obtainable in comparison to monolayer crystals of stearic acid and behenic acid. Large area crystals of the fatty acids have the tendency of being multilamellar.

In order to investigate whether monolayers tend to pack with extended unkinked chains, we present the comparison of observed structure factors for the major layer lines ($h = 0$, 1 and 5) from monolayer crystals to the calculated structure factors for a monolayer of monoclinic n-hexatriacontane [31] in Table 9. The monoclinic paraffin is used for comparison since its chain length is nearly the same as the wax chain. The R-factor for 14 ($hk0$) reflections

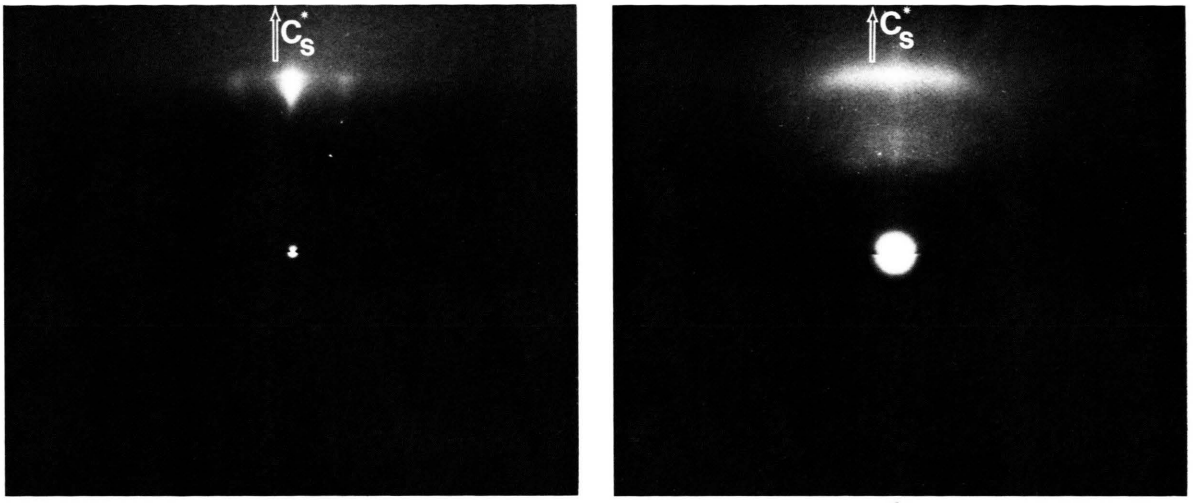

(a) (b)

Fig. 15. Reflection electron diffraction patterns: (a) orthorhombic n-hexatriacontane-single crystal, (b) behenic acid, form B — polycrystalline sample. Direction of c_s^* axis shown.

Table 9. Observed cetyl palmitate structure factors from oblique monolayer crystals vs. calculated values for n-hexatriacontane monoclinic monolayer [9] using only carbon positions and $B = 0.0$ Å^2.

$h\,k\,0$	$\lvert F_{obs}\rvert$	$n\,C_{36}$ monolayer $\lvert F_{calc}\rvert$	9 carbon pairs $\lvert F_{calc}\rvert$
020	5.77 *	6.75	6.75
040	2.79	2.47	2.47
060	1.10	0.33	0.33
080	0.65	0.48	0.48
110	0.76	0.61	0.72
120	0	0.14	0.21
130	0.64	0.33	0.36
140	0	0.16	0.21
150	0.43	0.11	0.10
160	1.51	1.91	1.91
520	0	0.04	0
530	0.44	1.26	1.26
540	0	0.05	0
550	0.55	0.51	0.51

* From average over patterns where linear response of film not exceeded.

is 0.28 and compares with the residual calculated for the $(h\,k\,0)_s$ reflections of the subcell upon tilting the crystals. In the structure factor calculation, no hydrogen contributions were considered, since these are generally used in the final stages of refinement in X-ray crystal structure analyses of long chain lipids (see Part I). Also no n-beam dynamical calculation was made for this zone. The phase grating calculation reported earlier [12] was probably an incorrect model for the dynamical diffraction from this projection since it did not account for phase shifts between successive subcell layers. Large cetyl palmitate crystals have been grown for a complete three-dimensional X-ray crystal structure analysis of this wax, and, thus, further computations of this type await the determination of accurate three-dimensional coordinates.

With these provisos in mind, Table 9 demonstrates that the relative intensities of $1\,k\,l$ reflections are comparable to those from an extended chain ($N \geqq 18$) but not those expected from short chain segments.

Discussion

The results reported here deal only with only chain crystals containing well defined methyl end planes. The reluctance for two layers to interact with each other can be understood from the relative energies of end plane interactions vs. side to side packing of long chains. For example, it has been long recognized that the lamination process of layers has been the growth limiting factor for crystals of this type [63]. Cleavage of crystals with an edge occurs very easily parallel to the {001} face but much less well normal to this face [64]. Differences in the methyl end planes account for the alteration of melting points for even and odd fatty acids. Sydow [65] calculated van der Waals attractive energies ($E = -n\,R^{-6}$) for a methyl group of two homologous acids for $R < 5.5$ Å. The C form gave a methyl end group attractive energy $E = -10.9$

$\times 10^{-4}$/methyl, the C′-form gave $E = -6.6 \times 10^{-4}$/methyl. On the same energy scale, a methylene group in a long chain has an attractive energy ($O_{\perp}$ methylene subcell), $E = -19.7 \times 10^{-4}$. More accurate quantitative potential energy calculations [66] on even n-paraffins based on lattice sums out to $R = 23$ Å, give a methylene contribution of -7.46 kJ/mol and a terminal methyl contribution of -11.46 kJ/mol. Considering that these latter methylene attractive potentials are additive for a long chain, the ratio per n-hexatriacontane molecule for methylene side interactions to methyl end group interactions is over 23:1. When translations along chain axes are important (e.g. the screw dislocation responsible for layer stacking and rumpling of surfaces) it is not difficult to imagine how difficult it is to fit two such layers, especially since the crystals are rapidly grown from evaporated solvent. The assumption of layer independence for a diffraction model is a logical consequence and has been corroborated by earlier experiment by Bassett *et al.* [67], in which paraffin crystal surfaces were decorated with gold. Quickly grown crystals always showed a greater surface decoration than slowly grown crystals, indicating a greater surface roughness in the former case. Stabilization of packing at greater crystal thickness also has been evidenced by the determination of c^* for cetyl palmitate from plotted rocking curves [12].

For the purposes of crystal structure analysis, it thus appears that rapidly-grown long chain crystals with flat methyl end planes will give electron diffraction intensities only from the methylene subcell. There is no doubt that bending contributes to this phenomenon to a large extent, but the paracrystalline nature of lipid packing seems to be another large factor in the isolation of layers from one another. Given the energetic arguments above, the greatest stabilization of a layer arises from the side to side packing of acyl chains. Small integral slips along the chain axes (screw dislocation) will not alter greatly this attractive interaction but it will severely distort the packing of both the polar regions and the methyl end planes. The latter distortion will cause the mismatch of the end planes-especially if there are *gauche* twists of the terminal bonds. Large shifts of this kind have been found for oblique layers [68] and the absence of coherent diffraction from polar regions indicates at least small shifts. Their possibility is indicated further by the existence of the screw dislocation growth. Reneker defects may exist in the center of the chain aggregate but the crystal structure analysis does not support the salient isolation of sublayers of methylene groups within an oblique monolayer.

This analysis does not hold for structures where end planes allow interdigitation of chain ends such that the methyl interface is spanned. Interactions are stronger and crystals grow easier in the c-direction. This phenomenon has been noted for superstructure forms of A-polymorph fatty acids [65], τ-form branched chain fatty acids [69], the tosylate of a diglyceride [70] and a phosphatidyl ethanolamine [71]. Electron diffraction patterns of the whole unit cell have been seen occasionally from needles of a phosphatidyl ethanolamine homologous to the compound determined by X-ray crystal structure analysis (Figure 16). Although original structure analyses based on interpretation of Patterson maps have assumed only a contribution from the methylene subcell [10] a later, independent direct phasing process [4] has a given potential map with a peak possibly due to a phosphorous atom in the polar moiety.

In the absence of large crystals, electron diffraction still offers the opportunity of obtaining (at

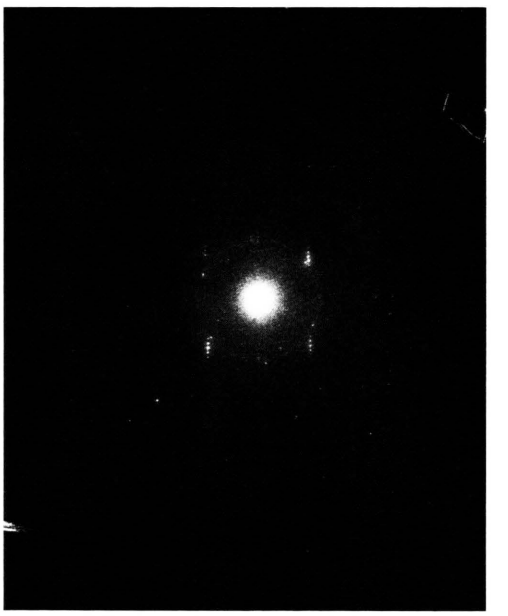

Fig. 16. Electron diffraction ($0kl$) pattern from 1,2-dipalmitoyl rac glycero-3-phosphoethanolamine needle showing true unit cell diffraction.

least) some quantitative information about the chain packing for unknown lipid crystal structures. The seldom used technique of reflection diffraction also has proved its efficiency again for polymethylene materials in determining chain axis tilt with respect to the crystal surface. It is indeed a necessary experiment for finding the required goniometer tilt to obtain an orientation with subcell (001) zone axis parallel to the incident beam.

Acknowledgements

The author is very grateful for the helpful criticism of this work by Professor John M. Cowley and technical assistance given by Miss C. M. Strozewski and Mr. Joseph Davis. Research was supported by Public Health Service Grant No. GM-21047 from the National Institute of General Medical Sciences, DHEW.

[1] B. K. Vainshtein, A. N. Lobachev, and M. M. Stasova, Soc. Phys. Crystallogr. **3**, 452 (1958).
[2] D. L. Dorset, Acta Crystallogr. **A 32**, 207 (1976).
[3] D. L. Dorset, J. Appl. Phys. **47**, 780 (1976).
[4] D. L. Dorset and H. A. Hauptman, Ultramicroscopy **1**, 195 (1976).
[5] D. L. Dorset and J. N. Turner, Naturwiss. **63**, 145 (1976).
[6] D. L. Dorset, Chem. Phys. Lipids **13**, 133 (1974).
[7] D. L. Dorset, Biochim. Biophys. Acta **380**, 257 (1975).
[8] S. W. Hui, D. F. Parsons, and M. Cowden, Proc. Nat. Acad. Sci. (US) **71**, 5068 (1974).
[9] D. L. Dorset, S. W. Hui, and C. M. Strozewski, J. Supramolec. Struct. **5**, 1 (1976).
[10] D. L. Dorset, Biochim. Biophys. Acta **424**, 396 (1976).
[11] D. L. Dorset, Chem. Phys. Lipids **14**, 291 (1975).
[12] D. L. Dorset, Bioorg. Khim. **2**, 781 (1976).
[13] D. L. Dorset, Naturwiss. **62**, 343 (1975).
[14] W. Buchheim and E. Knoop, Naturwiss. **56**, 560 (1969).
[15] E. Frede and D. Precht, Kieler Milchwirtschaftliche Forschungsber. **26**, 325 (1974).
[16] E. Knoop and D. Precht, Naturwiss. **62**, 37 (1975).
[17] D. Precht, Fette, Seifen, Anstrichmittel **78**, 145 (1976).
[18] J. M. Cowley, Acta Crystallogr. **14**, 920 (1961).
[19] E. S. Clark and L. T. Muus, Z. Krist. **177**, 108 (1962).
[20] B. K. Vainshtein, Diffraction of X-Rays by Chain Molecules, Elsevier, Amsterdam 1964, pp. 277–282.
[21] D. H. Reneker, B. M. Fanconi, and J. Mazur, J. Appl. Phys. **48**, 4032 (1977).
[22] E. O. Schlemper, W. C. Hamilton, S. J. La Placa, J. Chem. Phys. **5**, 3990 (1971).
[23] A. Hybl and D. L. Dorset, Acta Crystallogr. **B 27**, 977 (1971).
[24] L. H. Jensen and A. J. Mabis, Acta Crystallogr. **21**, 770 (1966).
[25] P. S. Doyle and P. S. Turner, Acta Crystallogr. **A 24**, 390 (1968).
[26] B. K. Vainshtein, Structure Analysis by Electron Diffraction, Pergamon, Oxford, p. 24 (1964).
[27] A. Müller, Proc. Roy. Soc. (London), **A 138**, 514 (1932).
[28] A. I. Kitaigorodskii, Organic Chemical Crystallography, Consultant's Bureau, New York, p. 187 (1961).
[29] P. W. Teare, Acta Crystallogr. **12**, 294 (1959).
[30] S. Amelinckx, Acta Crystallogr. **9**, 217 (1956).
[31] H. M. M. Shearer and V. Vand, Acta Crystallogr. **9**, 279 (1956).
[32] K. Larsson and E. von Sydow, Acta Chem. Scand. **20**, 1203 (1966).
[33] R. Kohlhaas, Z. Krist. **98**, 418 (1938).
[34] A. R. Verma and P. M. Reynolds, Proc. Phys. Soc. (London), **66 B**, 414 (1953).
[35] A. Keller, Phil. Mag. **6**, 329 (1961).
[36] D. C. Bassett and A. Keller, Phil. Mag. **6**, 345 (1961).
[37] E. F. Baltá Calleja, Rev. Acad. Cienc. Exact., Fis. Nat. Madrid, **50**, 71 (1965).
[38] I. M. Dawson and V. Vand, Proc. Roy. Soc. (London) **A 206**, 555 (1951).
[39] I. M. Dawson, Proc. Roy. Soc. (London), **A 214**, 72 (1952).
[40] A. W. Agar, F. C. Frank, and A. Keller, Phil. Mag. **4**, 32 (1959).
[41] V. F. Holland, P. H. Lindenmeyer, R. Trivedi, and S. Amelinckx, Phys. Stat. Sol. **10**, 543 (1965).
[42] M. Niinomi and M. Takayanagi, Progr. Polym. Sci. Japan **2**, 199 (1971).
[43] D. M. Sadler and A. Keller, Kolloid Z. u. Z. Polym. **239**, 641 (1970).
[44] J. R. White, J. Polym. Sci. — Physics **11**, 2173 (1973).
[45] J. R. White, J. Polym. Sci. — Physics **12**, 2375 (1974).
[46] V. F. Holland, J. Appl. Phys. **35**, 3235 (1964).
[47] V. F. Holland and P. H. Lindenmeyer, J. Appl. Phys. **36**, 3049 (1965).
[48] D. L. Dorset, J. Appl. Cryst. **9**, 142 (1976).
[49] A. R. Verma, Proc. Roy. Soc. (London) **A 228**, 34 (1955).
[50] S. Amelinckx, Acta Crystallogr. **8**, 530 (1955).
[51] D. L. Dorset, Naturwiss. **63**, 437 (1976).
[52] D. L. Dorset, Z. Naturforsch. **32 A**, 1166 (1977).
[53] J. M. Cowley and A. Goswami, Acta Crystallogr. **14**, 1071 (1961).
[54] J. M. Cowley, A. L. G. Rees, and J. A. Spink, Proc. Roy. Soc. (London), **A 64**, 609 (1958).
[55] D. H. Reneker, J. Polym. Sci. **59**, S 39 (1962).
[56] W. A. Pangborn, Ph. D. Thesis, University of Maryland School of Medicine (1973).
[57] S. Abrahamsson and B. Dahlén, Chem. Phys. Lipids **20**, 43 (1977).
[58] N. G. Guerina and B. M. Craven, Amer. Cryst. Assoc. Abstr., Ser. 2, **5**, 32 (1977).
[59] D. A. Langs, M. Erman, and G. T. De Titta, Science **197**, 1003 (1977).
[60] G. Strobl, B. Ewen, E. W. Fischer, and W. Piesczek, J. Chem. Phys. **61**, 5257 (1974).
[61] E. S. Clark and L. T. Muus, Z. Krist. **177**, 108 (1962).
[62] J. A. Chapman and D. Tabor, Proc. Roy. Soc. (London) **A 242**, 96 (1957).
[63] V. Daniel, Adv. Phys. **2**, 450 (1953).
[64] L. H. Jensen, J. Polym. Sci. **C 29**, 47 (1970).
[65] E. von Sydow, Ark. Kemi **9**, 231 (1956).
[66] H. E. L. Masden and R. Boistelle, Acta Crystallogr. **A 32**, 828 (1976).
[67] G. A. Bassett, D. J. Blundell, and A. Keller, J. Macromol. Sci. (Phys.) **B 1**, 161 (1967).
[68] B. Wunderlich and L. Melillo, Macromol. Chem. **118**, 250 (1968).
[69] S. Abrahamsson, Ark. Kemi **14**, 65 (1959).
[70] P. H. Watts, Jr., W. A. Pangborn, and A. Hybl, Science **175**, 60 (1972).
[71] P. B. Hitchcock, R. Mason, K. M. Thomas, and G. G. Shipley, Proc. Nat. Acad. Sci (US) **71**, 3036 (1974).